magnetochemistry

MDPI

Article

Magnetization Dynamics in Fe_xCo_{1-x} in Presence of Chemical Disorder

Banasree Sadhukhan [1,2,*], Raghuveer Chimata [3], Biplab Sanyal [3] and Abhijit Mookerjee [4]

1 KTH Royal Institute of Technology, AlbaNova University Center, SE-10691 Stockholm, Sweden
2 Department of Physics, Presidency University, 86/1 College Street, Kolkata 700073, India
3 Department of Physics and Astronomy, Uppsala University, Box 516, SE-75120 Uppsala, Sweden
4 S.N. Bose National Centre for Basic Sciences, JD-III, Salt Lake, Kolkata 700098, India
* Correspondence: banasree@kth.se

Abstract: In this paper, we present a theoretical formulation of magnetization dynamics in disordered binary alloys, based on the Kubo linear response theory, interfaced with a seamless combination of three approaches: density functional-based tight-binding linear muffin-tin orbitals, generalized recursion and augmented space formalism. We applied this method to study the magnetization dynamics in chemically disordered Fe_xCo_{1-x} (x = 0.2, 0.5, 0.8) alloys. We found that the magnon energies decreased with an increase in Co concentration. Significant magnon softening was observed in $Fe_{20}Co_{80}$ at the Brillouin zone boundary. Magnon–electron scattering increased with increasing Co content, which in turn modified the hybridization between the Fe and Co atoms. This reduced the exchange energy between the atoms and softened down the magnon energy. The lowest magnon lifetime was found in $Fe_{50}Co_{50}$, where disorder was at a maximum. This clearly indicated that the damping of magnon energies in Fe_xCo_{1-x} was governed by hybridization between Fe and Co, whereas the magnon lifetime was controlled by disorder configuration. Our atomistic spin dynamics simulations show reasonable agreement with our theoretical approach in magnon dispersion for different alloy compositions.

Keywords: chemical disorder; magnetization dynamics; alloy

Citation: Sadhukhan, B.; Chimata, R.; Sanyal, B.; Mookerjee, A. Magnetization Dynamics in Fe_xCo_{1-x} in Presence of Chemical Disorder. *Magnetochemistry* **2023**, *9*, 44. https://doi.org/10.3390/magnetochemistry9020044

Academic Editor: Carlos J. Gómez García

Received: 11 November 2022
Revised: 26 December 2022
Accepted: 21 January 2023
Published: 28 January 2023

1. Introduction

The dynamics and damping of magnetic excitations play a pivotal role in many modern day spintronic devices through the exploration of the nature of magnon dispersion and spin transport in pristine metals, semiconductors and their alloys. Band theory of ferromagnetism based on itinerant electrons has successfully predicted the magnetic properties of metallic systems, including transition metals, Heusler alloys and rare-earth magnets. However, these theoretical investigations have been a controversial subject for modern science due to the dual character of the d-electrons. Their ground state is described by the band-like itinerant electrons at $T = 0$. However, many open questions arise regarding the more general finite temperature ab initio approach, which includes spin excitation [1,2]. The spin wave theory of magnetism includes the fluctuations that switch from band theory of ferromagnetism to the spin dynamics approach [3–7].

A first principles study of the spin correlation function and magnon lifetimes of disordered magnetic systems has become important for both fundamental and technological interests. Recent advancements in experimental techniques have enabled us to probe magnon dynamics [8–15]. In a recent experiment using the spin-polarized electron energy loss spectroscopy (SPEELS) technique, it was shown that magnon energies were reduced (referred to as magnon softening) for a single ferromagnetic monolayer of Fe on W, compared with pure bulk Fe [16]. Theoretical predictions based on an itinerant electron model are in contradiction with the above experimental finding. Theoretical limitations have hindered a correct understanding of the fundamental nature of spin-wave excitations. The

structural relaxation between the Fe and W layers influences the hybridization between Fe and W states, which modifies the exchange interactions [17]. Disordered local moments (DLM) configuration reduces the exchange interaction strengths. This leads to significant magnon softening compared with bulk Fe. The magnetic ordering from Dzyaloshinskii–Moriya interactions (DMI), as a consequence of spin–orbit coupling, also leads to magnon softening. For the bulk system, these effects can be ignored.

Continuum and atomistic models have been developed to study spin dynamics in real materials. In micromagnetic simulations, a continuum model of magnetization is considered at a length scale much bigger than the interatomic distance [18]. Regarding atomistic models based on first principles methods, one may directly solve the time-dependent density functional equation, which requires huge computational cost and time to make realistic predictions for materials. The standard approach used to simulate the time evolution of the spin texture is to propagate the Landau–Lifshitz–Gilbert (LLG) equation [19,20]. However, the Hamiltonian required for solving the LLG equation contains several terms involving magnetic exchange and anisotropy. It should be mentioned that for a disordered magnetic alloy, the exchange interaction between atoms may strongly depend on the chemical composition [21–24]. Therefore, the magnon spectrum and lifetimes in a material depend on the configuration of the magnetic state via the local atomic environment [25]. Another important parameter in the LLG equation is the Gilbert damping parameter, which can be calculated by first principles electronic structure calculations. Two successful models in this regard are the breathing Fermi surface model (BFS) [26] and the torque correlation model (TCM) [27]. Unfortunately, neither of these models are parameter-free, nor do they really shed light on the microscopic origins of damping. Finally, it was found that damping arose from microscopic scattering processes [28–30]. Ebert et al. calculated the Gilbert damping parameter for the bcc Fe_xCo_{1-x} alloy from a CPA approach via linear response theory [30]. However, the microscopic origins of damping is still being uncovered.

The dynamical relaxation of various complex systems have also been a focus of considerable interest. In particular, spin relaxation in transition metal-based alloys have received considerable attention over the years. The relaxation time for ferromagnetic transition metals such as Fe, Co and Ni is strongly spin-dependent. The spin-averaged relaxation time in these metals is much shorter than in noble metals. The analysis of the peak-positions and broadening of magnon excitation provides us information on the magnon energy and lifetime, respectively. Magnon energy decays exponentially, such as exp(-γt/2$\hbar$), where γ represents the intrinsic line width of the Lorentzian peak in magnon spectral density and $\hbar$ is the reduced Plank constant. The magnon lifetime $\tau = 2\hbar/\gamma$ is usually defined as the time in which the amplitude drops to e^{-1} of its initial value. This is similar to the concept of a quantum mechanical broadening parameter and lifetime of an energy eigenstate [31–35].

The physical picture underlying the spin-dynamics method, which we present here, is not completely new, but their implementations in the presence of chemical and magnetic interactions within first principles accuracy are of fundamental importance. Augmented space formalism (ASF) has been successfully used to describe the effects of different disorders [36–46]. Here, we applied ASF for the simulation of spin dynamics, which enabled the characterization of magnetic excitations in the presence of chemical disorder within Kubo linear response formalism, in combination with a density functional-based first principles approach. The Hamiltonian parameters obtained from first principles theory provides a reliable tool for the analysis and even prediction of complex collective modes of magnetic materials. Our aim is to probe the magnon dynamics in chemically disordered Fe_xCo_{1-x} alloys.

This article is organized as follows: In Section 2, we describe the Hamiltonian for spin dynamics for binary alloys in the presence of chemical disorder. We use the augmented space recursion (ASR) approach to tackle the disordered Hamiltonian, techniques for the calculation of the adiabatic magnon lifetime and an atomistic scheme for the numerical integration of the equations of motion. We present computational details to describe the

dynamical spin response functions. Section 3 discusses the applicability of our method, taking bcc Fe as a testing ground, and results and discussions on Fe_xCo_{1-x}. Finally, our conclusions and research outlook are in Section 4 .

2. Methodology

2.1. Spin Transport at Low Temperatures

We analysed the spin transport in ferromagnetic alloys. We began with a ferromagnetic sea as our unperturbed state. A spin flip is an excitation or fluctuation in that state. We used the XXZ Heisenberg Hamiltonian with a random distribution of the exchange parameters in terms of creation and annihilation operators:

$$H = -\sum_{\vec{R}}\sum_{\vec{R}'} J(\vec{R}-\vec{R}')\left(a^{\dagger}_{\vec{R}}a_{\vec{R}'} + a^{\dagger}_{\vec{R}'}a_{\vec{R}} + \Delta\, \tilde{n}_{\vec{R}}\, \tilde{n}_{\vec{R}'}\right) \tag{1}$$

where Δ is the anisotropic exchange parameter describing the magnon–magnon interaction, $J(\vec{R}-\vec{R}')$ is the strength of the exchange interaction, $a^{\dagger}_{\vec{R}}$ and $a_{\vec{R}}$ are the magnon creation and annihilation operators, respectively, and $\tilde{n}_R = a^{\dagger}_{\vec{R}}a_{\vec{R}}$. The excitations in this model are described by spin waves or magnons that can be envisaged as spin patterns against a uniform spin background, moving on the underlying lattice. Here, we consider $\Delta \sim 0$, neglecting the magnon–magnon interaction within linear approximations.

The linear response to an external homogeneous disturbance was described in terms of two-particle Green's functions within the Kubo linear response theory [47]. If a spin system is disturbed by an external field that causes a perturbation in the XXZ Heisenberg Hamiltonian, then the spin response function $\Gamma(\vec{R}-\vec{R}', t-t')$ is related to the disturbance by a spin–spin correlation function $C(\vec{R}-\vec{R}', t-t')$ [47–49], which is given by:

$$\Gamma(\vec{R}-\vec{R}', t-t') = \frac{i}{\hbar}\Theta(t-t')\langle\Phi_0|[\sigma(\vec{R},t), \sigma(\vec{R}',t')]|\Phi_0\rangle$$

where $C(\vec{R}-\vec{R}', t-t') = \langle\Phi_0|[\sigma(\vec{R},t), \sigma(\vec{R}',t')]|\Phi_0\rangle$, $\sigma(\vec{R},t)$ is the spin operator, Θ is the Heaviside step function and $|\Phi_0>$ is the ground state. The dynamical structure factor $S(\vec{q},\omega)$ is the Laplace transform of the spin correlation function $C(\vec{R}-\vec{R}', t-t')$.

2.2. Recursive Approach to Dynamical Spin Response Functions

Our starting point was a dynamical variable described by the Hermitian operator $D(\vec{q},t)$, following the time evolution such that $|\Phi(t)\rangle = D(t)|\Phi_0\rangle$. Our guiding equation was the Kohn–Sham equation:

$$i\frac{\partial|\Phi(t)\rangle}{\partial t} = H|\Phi(t)\rangle$$

We followed the recursion procedure described by Gagliano and Balserio [50] and, Viswanathan and Muller [48,49,51,52]. We first chose a denumerable basis of representation $\{|\phi_n>\}$, and expanded the "wave function" on this basis:

$$|\Phi(t)\rangle = \sum_{n=1}^{\infty} D_n(\vec{q},t)|\phi_n\rangle \tag{2}$$

We began with $|\phi_1\rangle = a^{\dagger}(\vec{q})|\Phi_0\rangle$, where $a^{\dagger}(\vec{q}) = \frac{1}{\sqrt{N}}\sum_{\vec{R}} e^{-i\vec{q}\cdot\vec{R}}a^{\dagger}(\vec{R})$. In the next step, $|\phi_2\rangle = H|\phi_1\rangle - \alpha_1|\phi_1\rangle$ and orthogonality leads to $<\phi_1|\phi_2> = 0 \Rightarrow \alpha_1 = \frac{<\phi_1|H|\phi_1>}{<\phi_1|\phi_1>}$. Finally, for $n > 2$

$$|\phi_{n+1}>= H|\phi_n> -\alpha_n|\phi_n> -\beta_n^2|n-1>$$

orthogonality $< \phi_n|\phi_{n+1} >= 0 \Rightarrow \alpha_n = \frac{< \phi_n|H|\phi_n >}{< \phi_n|\phi_n >}$ $\beta_n^2 = \frac{< \phi_{n+1}|\phi_{n+1} >}{< \phi_n|\phi_n >}$. The $\{\alpha_n, \beta_n\}$ are the recursion parameters.

Substituting this into Equation (2), we get:

$$i\frac{\partial D_n(\vec{q},t)}{\partial t} = D_{n-1}(\vec{q},t) - \alpha_n D_n(\vec{q},t) - \beta_{n+1}^2 D_{n+1}(\vec{q},t)$$

Taking the Laplace transformation:

$$(z-\alpha_n)D_n(\vec{q},z) - i\delta_{n0} = D_{n-1}(\vec{q},z) + \beta_{n+1}^2 D_{n+1}(\vec{q},z)$$

where

$$D_0(\vec{q},z) = \cfrac{i}{z-\alpha_1 - \cfrac{\beta_1^2}{z-\alpha_2 - \cfrac{\beta_2^2}{z-\alpha_3 \ldots}}}$$

The dynamical structure factor is then

$$S(\vec{q},\omega) = \lim_{\delta\to 0} Re[D_0(\vec{q},\omega+i\delta)]$$

where $z = \omega + i\delta$.

2.3. Dynamical Spin Response Functions in the Presence of Disorder: The Augmented Space Approach

Then, we introduced disorder in the exchange parameters $J(\vec{R}-\vec{R}')$ by a set of random variables $\{n_{\vec{R}}\}$.

The randomness can be introduced in the exchange parameter through a local, binary random variable $n_{\vec{R}}$ ($\vec{R}$ can be occupied by an A or B type of atom for binary alloys), taking the values 0 and 1 with probabilities x and $y = 1-x$, respectively:

$$J(\vec{R}) = J^{AA}(\vec{R})n_{\vec{R}}n_{\vec{R}+\vec{x}} + J^{BB}(\vec{R})(1-n_{\vec{R}})(1-n_{\vec{R}+\vec{x}}) + J^{AB}(\vec{R})\Big(n_{\vec{R}}(1-n_{\vec{R}+\vec{x}}) + (1-n_{\vec{R}})n_{\vec{R}+\vec{x}}\Big)$$

where $\vec{R}' = \vec{R} + \vec{x}$.

The augmented space method [53–57] replaces these random variables $\{n_{\vec{R}}\}$ by operators $\{N_{\vec{R}}\}$. The eigenvalues are the random numbers taken by the variables $\{n_{\vec{R}}\}$ and the spectral functions are the probability densities of the operator $\{N_{\vec{R}}\}$ [58]. The augmented space is an outer product of real space $\Phi_{\vec{R}}$ (lattice space) and configuration space $\{\emptyset\}$ (random space). Then, the configuration (disorder) averaged spin response function was given by:

$$\ll \Gamma(\vec{q},z) \gg \quad = \quad \langle \Phi_{\vec{q}} \otimes \{\emptyset\}|(z\tilde{I} - \tilde{H})^{-1}|\Phi_{\vec{q}} \otimes \{\emptyset\}\rangle$$

where $\tilde{H}$ is the disordered Hamiltonian.

Now, the configuration-averaged dynamical operator in the disordered system can be expressed as a continued fraction of recursion coefficients $\{\tilde{\alpha}_n, \tilde{\beta}_n\}$, as:

$$\ll D_0(\vec{q},z) \gg = \cfrac{i}{z-\tilde{\alpha}_1 - \cfrac{\tilde{\beta}_1^2}{z-\tilde{\alpha}_2 - \cfrac{\tilde{\beta}_2^2}{z-\tilde{\alpha}_3 \ldots}}}$$

Then, the configuration-averaged dynamical structure factor was obtained by:

$$\ll S(\vec{q},\omega) \gg = \lim_{\delta \to 0} Re \ll D_0(\vec{q},\omega + i\delta) \gg$$

The self-energy $\Sigma(\vec{q},z)$, via the recursion method suggested by Viswanath and Müller [48,49,51,52], was given by:

$$\Sigma(\vec{q},z) = \cfrac{\tilde{\beta}_2^2}{z - \tilde{\alpha}_2 - \cfrac{\tilde{\beta}_3^2}{z - \tilde{\alpha}_3 - \cfrac{\tilde{\beta}_4^2}{\ddots\, z - \tilde{\alpha}_n - \tilde{\beta}_n^2 T(\vec{q},z)}}}$$

The terminator $T(\vec{q},z)$, which reflects all the singularities in the response function, was constructed from the calculated $\{\tilde{\alpha}_n, \tilde{\beta}_n\}$ for $n = 1, \ldots N$ [52,59–63]. Therefore, we used the square-root terminator [60,61] with the calculated recursion coefficients to taken into account the convergence of the continued fraction. $\mathrm{Im}[\Sigma(\vec{q},\omega)]$ counts the disorder-induced broadening, which provides the disorder-induced lifetime τ of the magnon state by $\mathrm{Im}[\Sigma(\vec{q},\omega)] = 1/\tau(\vec{q})$

We studied the configuration-averaged dynamical response function of chemically disordered binary alloys, using ASR within Kubo linear response theory [53–57]. The ASR technique went beyond the usual single-site mean-field coherent potential approximation (CPA)-like approach to study the environmental effects for chemically disordered alloys. In particular, the methodology we implemented here was an admixture of the tight binding linear muffin-tin orbitals (TB-LMTO) technique, ASF and generalized recursion (GR) [48,49,51,64]. This provided an accurate computational framework for analysing dynamical response properties.

We calculated the configuration-averaged dynamical structure factors $\ll S(\vec{q},\omega) \gg$ of Fe_xCo_{1-x} for three different Co contents (x = 0.2, 0.5, 0.8). This relates the response of the systems in the presence of an external perturbation (in our case, chemical disorder) from the self-energy. We also calculated the magnon lifetime $\tau(\vec{q})$ of Fe_xCo_{1-x}. The Brillouin zone boundary in the [001] direction of FeCo was nearly 2 $Angstrom^{-1}$. We neglected the effects of magnon–magnon and magnon–stoner interactions. We focused on the magnon–electron interactions to study the effects of chemical disorder on Fe_xCo_{1-x}.

2.4. Atomistic Spin Dynamics

To compare our results, we also calculated the magnon dispersion spectra of Fe_xCo_{1-x} (x = 0.2, 0.5, 0.8) from the Uppsala Atomistic Spin Dynamics (UppASD) code [6,7]. The necessary exchange parameters for UppASD were calculated in the the framework of *ab-initio* density functional theory (DFT). These were performed by means of the Korringa–Kohn–Rostocker Green's function formalism, as implemented in the SPRKKR package [65]. The shape of the potential was treated by the atomic sphere approximation (ASA), whereas relativistic effects were considered by taking the fully relativistic Dirac equation. The effect of the exchange correlation part of the energy was treated by considering the generalized gradient approximation (GGA), as devised by Perdew, Burke and Ernzerhof [66]. Substitutional disorder between sub-lattices could also be studied by making the use of the CPA. Interatomic exchange interactions were calculated via the LKAG formalism [67].

The UppASD code [68] is based on the framework of LLG formalism. The temporal evolution of an atomic moment in LLG formalism is given by:

$$\frac{d\mathbf{m_i}(t)}{dt} = -\frac{\gamma}{1+\alpha^2}\mathbf{m_i}(t) \times [\mathcal{H}^{\mathbf{i}}_{\mathbf{eff}} + \frac{\alpha}{m_s}\,(\mathbf{m_i}(t) \times \mathcal{H}^{\mathbf{i}}_{\mathbf{eff}})]$$

where $\mathbf{m_i}(t)$ is the atomic moment on the i'th site at time t. γ is the gyromagnetic ratio and α is the Gilbert damping factor, which we have assumed to be 3×10^{-4}. m_s is the saturation moment for the i'th atom. The temperature effect in ASD was measured using a stochastic

magnetic field, included in the term of effective field $\mathcal{H}^{\mathbf{i}}_{\mathbf{eff}}$. The effective field $\mathcal{H}^{\mathbf{i}}_{\mathbf{eff}}$ on the i'th atom is calculated from the effective magnetic Hamiltonian given by

$$\mathcal{H}_{Mag} = \mathcal{H}_{ex}$$

through

$$\mathcal{H}^{\mathbf{i}}_{\mathbf{eff}} = -\frac{\partial \mathcal{H}_{Mag}}{\partial \mathbf{m}_i(t)}.$$

$\mathcal{H}_{ex}$ describes the magnetic exchange interactions between the spins. $\mathcal{H}_{Mag}$ is given by

$$\mathcal{H}_{Mag} = \sum_{i,j} J_{ij} \mathbf{S}_i \cdot \mathbf{S}_j$$

In order to calculate magnon dispersion relation, one should calculate spin–spin correlation function. The spin–spin correlation in an effective field is obtained by solving the LLG equation and can be written as:

$$C(R - R', t) = \langle m_R(t) m_{R'}(0) \rangle - \langle m_R(t) \rangle \langle m_{R'}(0) \rangle$$

where the ensemble average is represented in angular brackets and k is the Cartesian component. The Fourier transform of the spin–spin correlation function, known as the dynamical structure factor, is written as:

$$S(\vec{q}, \omega) = \frac{1}{\sqrt{2\pi N}} \sum_{R,R'} \int_{-\infty}^{\infty} e^{i\omega t} C(R - R', t) dt$$

$S(\vec{q}, \omega)$ is measured in neutron-scattering experiments.

3. Results and Discussion

Before studying the magnetization dynamics in Fe_xCo_{1-x}, we investigated the charge distribution of a body-centered, disordered $Fe_{50}Co_{50}$ alloy. We compared the disordered alloy with a corresponding ordered, B2-structured alloy. In Table 1, we show the chemical effects of disorder and the redistribution of charge upon alloying. In these alloys, there was a small decrease of sp-like charges and a corresponding small increase in the d-like channel in both Fe and Co. These effects were small, with the introduction of disorder. The magnetocrystalline anisotropy is the energy difference between the magnetic ground state, when the magnetic quantization (spin) axis is along the easy axis (which is along the c-axis for FeCo) and along the easy plane (which is the ab-plane for FeCo), i.e., $K^u = E^c - E^{||}$. Bulk FeCo has $\frac{c}{a} \sim 1$ without any tetragonal distortion. Therefore, we ignored the effects of single-ion anisotropy in FeCo alloys.

Table 1. Charge redistribution upon alloying: distribution for the ordered B2 and disordered body-centered cubic (BCC) structures for the 50-50 FeCo alloy. The charge is given in units of electronic charge e.

Alloy Component	**Fe**			**$Fe_{0.5}Co_{0.5}$** **Co**		
Atomic radius	R_0 = 2.64 Å			R_0 = 2.60 Å		
Charge	*sp*	*d*	Tot	*sp*	*d*	Tot
Atomic state	2.0	6.0	8.0	2.0	7.0	9.0
B2 ordered	1.44	6.52	7.96	1.46	7.58	9.04
BCC disordered	1.43	6.55	7.99	1.43	7.63	9.06

We were interested in calculating the ensemble-averaged dynamical structure factor $\ll S(\vec{q},\omega) \gg$ to understand the magnetization dynamics in disordered Fe_xCo_{1-x} alloys. Figure 1a–c shows the momentum-resolved dynamical structure function $\ll S(\vec{q},\omega) \gg$, convoluted with a Lorenzian function with three disorder concentrations (x = 0.2, 0.5, 0.8) along the symmetric $\Gamma - H$ direction. Irrespective of the disorder concentration, for low $\vec{q}$ values, the spectral intensity, estimated from the peak value of the Lorenztian, was high. The spectral intensity dropped to minimum values for intermediate $\vec{q}$, after which it again rose with increasing $\vec{q}$. At the same time, the peak width monotonically increased with increasing energy, as well as wave vectors ($\vec{q}$). The broadening of the peak in $\ll S(\vec{q},\omega) \gg$ for larger $\vec{q}$ values came from a magnon–electron scattering mechanism due to chemical impurity. The itinerant collective excitations of spin waves (magnon) lost their energy as a consequence of chemical disorder. A large damping of magnons in the tetragonally distorted bulk FeCo compound was also previously predicted [69,70].

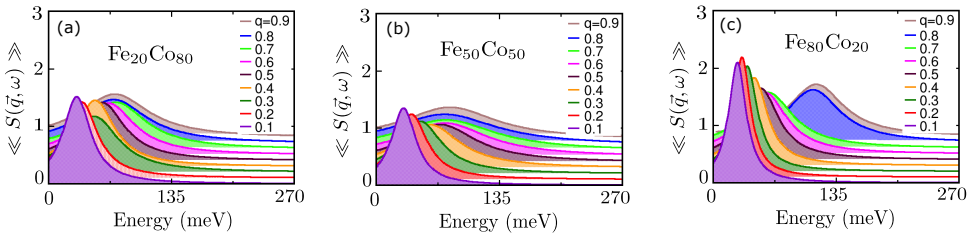

Figure 1. The dynamical structure factors $\ll S(\vec{q},\omega) \gg$ for a selection of wave vectors $\vec{q}$, varying from 0.1 to 0.9 along the symmetric $\Gamma - H$ direction in the Brillouin zone of bcc Fe_xCo_{1-x} alloys with (**a**) $x = 0.2$, (**b**) $x = 0.5$ and (**c**) $x = 0.8$, respectively. In order to identify the peak position, the dynamical structure function $\ll S(\vec{q},\omega) \gg$ was convoluted with a Lorentzian function, normalized to unity.

Here, we elaborate on the technique of peak finding from $\ll S(\vec{q},\omega) \gg$. After configuration averaging, in order to identify the position of the intensity peaks of the dynamical structure factor $\ll S(\vec{q},\omega) \gg$, we convoluted the respective intensity profiles of $\ll S(\vec{q},\omega) \gg$ for each $\vec{q}$ vector with a Lorentzian function, normalized to unity. In order to justify this technique, we applied it to calculate magnon dispersion of the bulk bcc Fe (see Figure 2a). This was to show that the implemented technique was able to qualitatively predict our experimental findings.

Then, we employed a different technique for the chemically disordered Fe_xCo_{1-x} alloys. We calculated the magnon dispersion of disordered Fe_xCo_{1-x} alloys along the $\Gamma - H$ direction, and studied the effects of chemical disorder on it. We found quadratic dependence upon $\vec{q}$ for the spin wave spectrum of magnon, as shown in Figure 2b. Bulk Fe had a steeper magnon dispersion compared with the disordered structure. This was expected due to the absence of magnon–electron scattering in the disorder-free material. The interesting point to note here is that the steepness of magnon energy gradually decreased with increasing Co concentration. $Fe_{80}Co_{20}$ exhibited higher magnon velocity for weaker scattering effects, and vice versa.

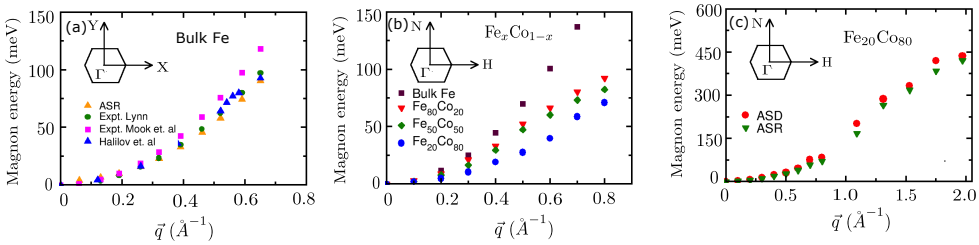

Figure 2. (**a**) Magnon dispersion spectrum for bulk bcc Fe along the $\Gamma - Y$ direction from ASR. For comparison, the experimental spin-wave spectrum of bulk bcc Fe by Lynn (Ref. [71]) and data from another experimental study corresponding to a spin-wave stiffness constant of D = 280 Å^2 by Mook et al. (Ref. [72]) are displayed. The blue triangles represent theoretical data by Halilov et al. (Ref. [73]). All comparisons were consistent with with the data from ASR [72]. (**b**) Magnon dispersion spectrum for bulk bcc Fe_xCo_{1-x} alloys along the high symmetric $\Gamma - H$ direction in the Brillouin zone for three different Co concentrations from ASR. This shows magnon softening in the $Fe_{20}Co_{80}$ alloy, compared with the others. (**c**) Magnon dispersion spectra for disordered $Fe_{20}Co_{80}$ from ASR and ASD.

The magnon softening is clearly visible in $Fe_{20}Co_{80}$ at the zone boundary. This is due to the fact that magnon–electron scattering modifies the exchange energy between Fe and Co moments. The chemical disorder between the Fe and Co atoms influenced the hybridization between Fe and Co states, which reduced the exchange interactions. This is shown in Table 2. The strength of exchange interaction for Fe_xCo_{1-x} gradually decreased with increasing Co content. This clearly indicates the softening of Fe_xCo_{1-x} with increasing Co content. The chemical disorder between Fe and Co also increased damping, which enhanced magnon softening. Ebert et al. calculated the Gilbert damping parameter from first principles theory for bcc Fe_xCo_{1-x} alloys [30]. Damping was at a minimum for 20% Co content and gradually increased with increasing Co content. This led to strong magnon softening in the $Fe_{20}Co_{80}$ alloy. Our results are also consistent with an experiment by Oogane et al. on bcc Fe_xCo_{1-x} alloys [74].

Table 2. The calculated nearest-neighbour exchange parameters in the framework of ab-initio density functional theory using the Korringa–Kohn–Rostocker Green's function formalism, implemented in the SPRKKR package [65].

Alloy	Fe-Fe (meV)	Fe-Co (meV)	Co-Co (meV)
$Fe_{80}Co_{20}$	2.065	2.302	1.740
$Fe_{50}Co_{50}$	2.083	2.117	1.418
$Fe_{20}Co_{80}$	1.919	1.880	1.208

For completeness, we also computed the magnon dispersion spectrum along the $\Gamma - H$ direction in the Brillouin zone. We compared the magnon spectra of disordered $Fe_{20}Co_{80}$ between ASR and ASD, taking the first nearest-neighbour exchange interaction into consideration (as shown in Figure 2c). The ASD simulations were performed with a system size of $120 \times 120 \times 120$ at a temperature of 0.1 K. ASD followed similar characteristic behavior with increasing Co concentrations. It was observed that the softening became stronger near the zone boundary (higher $\vec{q}$ values). The steepness of dispersion reduced as magnon–electron scattering increased. It was also observed in the profile of $\ll S(\vec{q}, \omega) \gg$ in Figure 1a. Both the numerical techniques exhibited the same effect.

To justify our results further, we performed ASD simulations for the nearest neighbour (Figure 3a–c) and 12 neighbor exchange interactions (Figure 3d–f). The qualitative features in the magnon spectra for the first and 12 neighbor shells were similar. The softening of the magnon spectra for the $Fe_{20}Co_{80}$ alloy was similar to that obtained from the ASR calculations as shown in Figure 2c. Additionally, we observed some branching in dispersion along $H - N$ for higher Co concentrations. A stronger tendency for branching was visible

at the N point of the Brillouin zone. However, we focused only on the magnon softening in $\Gamma - H$ direction. This strong magnon softening was in contradiction with a previous study based on an itinerant electron model at $T = 0$ K [75,76]. Our findings present the possibility that a disordered Fe_xCo_{1-x} may not be a simple itinerant ferromagnet. The effects of spin correlations are important for this system. This behaviour is commonly interpreted as a transition from conductivity-like behaviour. This reflects the dominance of intra- and interband transitions. This is related to the broadening of electron energy bands caused by an increase in scattering events with concentrations of Co. An increase in the Co content in Fe_xCo_{1-x} led to more impurity-scattering. This was responsible for band broadening, which increased the damping of magnon. This effect completely suppressed the conductivity-like behaviour in the low-temperature regime, and increased scattering due to chemical disorder.

The broadening of the magnon excitation peak ($\ll S(\vec{q},\omega) \gg$) provides a way to calculate the magnon lifetime τ. The Fourier transform of the Lorentzian in the energy (or frequency) domain is an exponential decay of magnon lifetime, such as $\exp(-t\Gamma/2\hbar)$, where Γ represents the intrinsic linewidth of the Lorentzian peak in energy and $\hbar$ is the reduced Planck constant. The relaxing magnetic modes or patterns are labelled by $\vec{q}$, such that the average 'size' of the mode is $O(q^{-1})$. We obtained the magnon lifetimes from the Fourier transform of the configuration-averaged correlation function. The large broadening of $\ll S(\vec{q},\omega) \gg$ yielded a small relaxation time, which clearly indicated strong scattering. Figure 3g shows the lifetime τ for Fe_xCo_{1-x} (x = 0.8, 0.5, 0.2) as a function of $\vec{q}$ ($Angstrom^{-1}$). We found the minimum magnon lifetime in $Fe_{50}Co_{50}$. This confirmed that the disorder was at a maximum in 50-50 configurations where $\ll S(\vec{q},\omega) \gg$ became maximally broadened for higher $\vec{q}$ values (see Figure 1b. Therefore, the magnon lifetime was not governed by hybridization between Fe and Co, but rather controlled by disorder configuration.

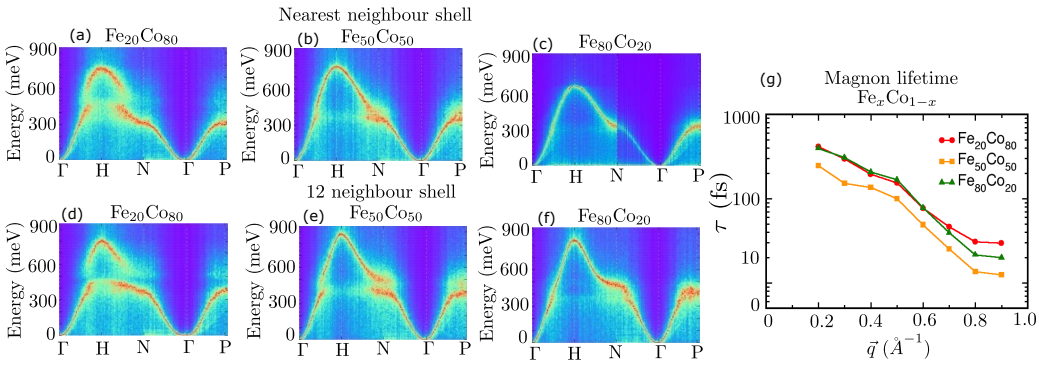

Figure 3. The figures in the top row (**a**–**c**) show the magnon dispersion of Fe_xCo_{1-x} (where x = 0.2, 0.5 and 0.8) alloys with nearest-neighbour exchange parameters and the bottom row figures show the plots (**d**–**f**) with the 12 neighbour shell exchange parameters. (**g**) Magnon lifetimes for disordered Fe_xCo_{1-x} alloys for x = 0.2, 0.5 and 0.8 from ASR.

In the current study, we propose using the ASR technique to study magnetization dynamics in chemically disordered alloys (which could also be generalised to surfaces and interfaces) and compare calculated magnon energy spectra with ASD-simulated magnon spectra. There are two different approaches within first principles theory for studying magnetization dynamics in materials: ASR and ASD. These approaches are based on two different working principles. ASD is based on the LLG theory, whereas the ASR based on the Kubo linear response theory. ASR captures the effect of hybridization between Fe and Co on the magnon softening of $Fe_{20}Co_{80}$ alloys (see Figure 2c), as well as magnon lifetimes in chemically disordered alloys originating from magnon band broadening (see Figure 3g).

4. Conclusions

In conclusion, we have investigated magnetization dynamics in the presence of chemical disorder using a first principles TB-LMTO-ASR method, interfaced with Kubo linear

response theory. This serves as a general and powerful computational tool for studying the effect of chemical disorder on magnetic excitations in binary random alloys. We applied our technique to study the magnetization dynamics in disordered Fe_xCo_{1-x} alloys, which are of great fundamental and technological interest [77–80]. We showed that the magnon–electron scattering mechanism plays a crucial role in determining the exchange interaction between Fe and Co. Magnon softening increases with Co concentration as the exchange interaction decreases. Our findings were further supported by atomistic spin dynamics simulations. Moreover, we calculated magnon lifetimes from the broadening widths of dynamical structure factors. It was found that the maximally disordered alloy showed the smallest lifetime. Therefore, magnon softening depends on the hybridization between Fe and Co, whereas the magnon lifetime depends on the disorder configuration. The proposed formalism could be used to study the magnetization dynamics in any binary random alloy.

Author Contributions: Conceptualization, A.M. (The project was originally conceived by Abhijit Mookerjee (A.M).) and B.S. (Banasree Sadhukhan); methodology, A.M. and B.S. (Banasree Sadhukhan); validation, B.S. (Banasree Sadhukhan), R.C. and B.S. (Biplab Sanyal); formal analysis, B.S. (Banasree Sadhukhan); investigation, B.S. (Banasree Sadhukhan); resources, B.S. (Banasree Sadhukhan); data curation, B.S. (Banasree Sadhukhan); writing—original draft preparation, B.S. (Banasree Sadhukhan); writing—review and editing, B.S. (Banasree Sadhukhan) and B.S. (Biplab Sanyal).; visualization, B.S. (Banasree Sadhukhan); supervision, A.M. All authors have read and agreed to the published version of the manuscript.

Funding: This research received no external funding.

Informed Consent Statement: Not applicable.

Data Availability Statement: The data supporting for the present study are available from the corresponding author upon request.

Conflicts of Interest: The authors declare no conflict of interest.

References

1. Moriya, T. *Electron Correlation and Magnetism in Narrow-Band Systems: Proceedings of the Third Taniguchi International Symposium, Mount Fuji, Japan, November 1–5. 1980*; Springer Science, Business Media: Berlin/Heidelberg, Germany, 2012; Volume 29.
2. Moriya, T.; Hasegawa, H. A Unified Theory of Magnetism in Narrow Band Electron Systems. *J. Phys. Soc. Jpn.* **1980**, *48*, 1490. [CrossRef]
3. Antropov, V.P.; Katsnelson, M.I.; Harmon, B.N.; van Schilfgaarde, M.; Kusnezov, D. Spin dynamics in magnets: Equation of motion and finite temperature effects. *Phys. Rev. B* **1996**, *54*, 1019. [CrossRef] [PubMed]
4. Nowak, U.; Mryasov, O.N.; Wieser, R.; Guslienko, K.; Chantrell, R. Spin dynamics of magnetic nanoparticles: Beyond Brown's theory *Phys. Rev. B* **2005**, *72*, 172410. [CrossRef]
5. Hellsvik, J.; Thonig, D.; Modin, K.; Iusan, D.; Bergman, A.; Eriksson, O.; Bergqvist, L.; Delin, A. General method for atomistic spin-lattice dynamics with first-principles accuracy. *Phys. Rev. B* **2019**, *99*, 104302. [CrossRef]
6. Eriksson, O.; Bergman, A.; Bergqvist, L.; Hellsvik, J. *Atomistic Spin Dynamics: Foundations and Applications*; Oxford University Press: Oxford, UK, 2017.
7. Skubic, B.; Hellsvik, J.; Nordström, L.; Eriksson, O. A method for atomistic spin dynamics simulations: implementation and examples. *J. Phys. Condens. Matter* **2008**, *20*, 315203. [CrossRef]
8. Dalosto, S.; Riera, J. Magnetic order in ferromagnetically coupled spin ladders. *Phys. Rev. B* **2000**, *62*, 928. [CrossRef]
9. Hopster, H. Spin-polarized electron energy loss spectroscopy. *Surf. Rev. Lett.* **1994**, *1*, 89. [CrossRef]
10. Vollmer, R.; Etzkorn, M.; Kumar, P.S.A.; Ibach, H.; Kirschner, J. Spin-Polarized Electron Energy Loss Spectroscopy of High Energy, Large Wave Vector Spin Waves in Ultrathin fcc Co Films on Cu(001). *Phys. Rev. Lett.* **2003**, *91*, 147201. [CrossRef] [PubMed]
11. Vollmer, R.; Etzkorn, M.; Kumar, P.A.; Ibach, H.; Kirschner, J. Spin-wave excitation observed by spin-polarized electron energy loss spectroscopy: a new method for the investigation of surface- and thin-film spin waves on the atomic scale. *Thin Solid Films* **2004**, *464*, 42. [CrossRef]
12. Vollmer, R.; Etzkorn, M.; Kumar, P.A.; Ibach, H.; Kirschner, J. Spin-polarized electron energy loss spectroscopy: A method to measure magnon energies. *J. Magn. Magn. Mater.* **2004**, *272*, 2126. [CrossRef]
13. Zhang, Y.; Chuang, T.-H.; Zakeri, K.; Kirschner, J. Relaxation Time of Terahertz Magnons Excited at Ferromagnetic Surfaces. *Phys. Rev. Lett.* **2012**, *109*, 087203. [CrossRef] [PubMed]
14. Zakeri, K.; Zhang, Y.; Chuang, T.-H.; Kirschner, J. Magnon Lifetimes on the Fe(110) Surface: The Role of Spin-Orbit Coupling. *Phys. Rev. Lett.* **2012**, *108*, 197205. [CrossRef] [PubMed]

15. Zakeri, K.; Zhang, Y.; Kirschner, J. Surface magnons probed by spin-polarized electron energy loss spectroscopy. *J. Electron Spectrosc. Relat. Phenom.* **2013**, *189*, 157. [CrossRef]
16. Prokop, J.; Zhang, Y.; Tudosa, I.; Peixoto, T.R.F.; Zakeri, K.; Kirschner, J. Magnons in a Ferromagnetic Monolayer *Phys. Rev. Lett.* **2009**, *102*, 177206. [CrossRef]
17. Bergman, A.; Taroni, A.; Bergqvist, L.; Hellsvik, J.; Hjörvarsson, B.; Eriksson, O. Magnon softening in a ferromagnetic monolayer: A first-principles spin dynamics study *Phys. Rev. B* **2010**, *81*, 144416. [CrossRef]
18. Fidler, J.; Schrefl, T. Micromagnetic modelling - the current state of the art. *J. Phys. D Appl. Phys.* **2000**, *33*, R135. [CrossRef]
19. Krieger, K.; Dewhurst, J.; Elliott, P.; Sharma, S.; Gross, E. Laser-Induced Demagnetization at Ultrashort Time Scales: Predictions of TDDFT. *J. Chem. Theory Comput.* **2015**, *11*, 4870. [CrossRef]
20. Gilbert, T.L. A phenomenological theory of damping in ferromagnetic materials. *IEEE Trans. Magn.* **2004**, *40*, 3443. [CrossRef]
21. Shimizu, M. Itinerant electron magnetism. *Rep. Prog. Phys.* **1981**, *44*, 329. [CrossRef]
22. Sabiryanov, R.F.; Bose, S.K.; Mryasov, O.N. Effect of topological disorder on the itinerant magnetism of Fe and Co. *Phys. Rev. B* **1995**, *51*, 8958. [CrossRef]
23. Sabiryanov, R.F.; Jaswal, S.S. Magnons and Magnon-Phonon Interactions in Iron. *Phys. Rev. Lett.* **1999**, *83*, 2062. [CrossRef]
24. Bonetti, S.; Hoffmann, M.C.; Sher, M.-J.; Chen, Z.; Yang, S.-H.; Samant, M.G.; Parkin, S.S.P.; Dürr, H.A. THz-Driven Ultrafast Spin-Lattice Scattering in Amorphous Metallic Ferromagnets. *Phys. Rev. Lett.* **2016**, *117*, 087205. [CrossRef] [PubMed]
25. Sadhukhan, B.; Bergman, A.; Kvashnin, Y. O. ; Hellsvik, J.; Delin, A. Spin-lattice couplings in two-dimensional CrI_3 from first-principles computations *Phys. Rev. B* **2022**, *105*, 104418. [CrossRef]
26. Kamberskỳ, V. On the Landau–Lifshitz relaxation in ferromagnetic metals. *Can. J. Phys.* **1970**, *48*, 2906. [CrossRef]
27. Kamberskỳ, V. On ferromagnetic resonance damping in metals. *Czechoslov. J. Phys. B* **1976**, *26*, 1366. [CrossRef]
28. Brataas, A.; Tserkovnyak, Y.; Bauer, G.E. Scattering Theory of Gilbert Damping. *Phys. Rev. Lett.* **2008**, *101*, 037207. [CrossRef] [PubMed]
29. Liu, Y.; Starikov, A.A.; Yuan, Z.; Kelly, P.J. First-principles calculations of magnetization relaxation in pure Fe, Co, and Ni with frozen thermal lattice disorder. *Phys. Rev. B* **2011**, *84*, 014412. [CrossRef]
30. Ebert, H.; Mankovsky, S.; Ködderitzsch, D.; Kelly, P.J. Ab Initio Calculation of the Gilbert Damping Parameter via the Linear Response Formalism. *Phys. Rev. Lett.* **2011**, *107*, 066603. [CrossRef]
31. Hong, X.; Zou, K.; Zhu, J. Quantum scattering time and its implications on scattering sources in graphene. *Phys. Rev. B* **2009**, *80*, 241415. [CrossRef]
32. Hwang, E.H.; Sarma, S.D. Single-particle relaxation time versus transport scattering time in a two-dimensional graphene layer. *Phys. Rev. B* **2008**, *77*, 195412. [CrossRef]
33. Das, B.; Subramaniam, S.; Melloch, M.R.; Miller, D.C. Single-particle and transport scattering times in a back-gated $GaAs/Al_xGa_{1-x}As$ modulation-doped heterostructure. *Phys. Rev. B* **1993**, *47*, 9650. [CrossRef] [PubMed]
34. Sadhukhan, B.; Bandyopadhyay, S.; Nayak, A.; Mookerjee, A. Disorder induced lifetime effects in binary disordered systems: A first principles formalism and an application to disordered graphene. *Int. J. Mod. Phys. B* **2017**, *31*, 1750218. [CrossRef]
35. Sadhukhan, B.; Zhang, Y.; Ray, R.; van den Brink, J. First-principles calculation of shift current in chalcopyrite semiconductor $ZnSnP_2$. *Phys. Rev. Mater.* **2020**, *4*, 064602. [CrossRef]
36. Saha, T.; Mookerjee, A. The effects of local lattice distortion in non-isochoric alloys: CuPd and CuBe. *J. Phys. Condens. Matter* **1996**, *8*, 2915. [CrossRef]
37. Kaphle, G.C.; Adhikari, N.; Mookerjee, A. Study of Spin Glass Behavior in Disordered Pt_xMn_{1-x} Alloys: An Augmented Space Recursion Approach. *Adv. Sci. Lett.* **2015**, *21*, 2681. [CrossRef]
38. Alam, A.; Mookerjee, A. Ab initio electronic structure calculation of disorder ternary alloys: A reciprocal-space formulation. *Phys. Rev. B* **2010**, *81*, 184205. [CrossRef]
39. Ganguly, S.; Venkatasubramanian, A.; Tarafder, K.; Dasgupta, I.; Mookerjee, A. Augmented space recursion study of the effect of disorder on superconductivity. *Phys. Rev. B* **2009**, *79*, 224204. [CrossRef]
40. Rahaman, M.; Mookerjee, A. Augmented-space cluster coherent potential approximation for binary random and short-range ordered alloys. *Phys. Rev. B* **2009**, *79*, 054201. [CrossRef]
41. Alam, A.; Saha-Dasgupta, T.; Mookerjee, A.; Chakrabarti, A.; Das, G.P. Electronic structure and phase stability of disordered hexagonal close-packed alloys. *Phys. Rev. B* **2007**, *75*, 134203. [CrossRef]
42. Alam, A.; Ghosh, S.; Mookerjee, A. Phonons in disordered alloys: Comparison between augmented-space-based approximations for configuration averaging to integration from first principles. *Phys. Rev. B* **2007**, *75*, 134202. 75.134202. [CrossRef]
43. Saha, T.; Dasgupta, I.; Mookerjee, A. Augmented-space recursive method for the study of short-ranged ordering effects in binary alloys. *Phys. Rev. B* **1994**, *50*, 13267. [CrossRef]
44. Sadhukhan, B.; Singh, P.; Nayak, A.; Datta, S.; Johnson, D.D.; Mookerjee, A. Band-gap tuning and optical response of two-dimensional Si_xC_{1-x} : A first-principles real-space study of disordered two-dimensional materials *Phys. Rev. B* **2017**, *96*, 054203. [CrossRef]
45. Sadhukhan, B.; Nayak, A.; Mookerjee, A. Effect of disorder on the optical response of NiPt and Ni_3Pt alloys. *Comput. Mater. Sci.* **2017**, *140*, 1. [CrossRef]

46. Sadhukhan, B.; Nayak, A.; Mookerjee, A. Effect of random vacancies on the electronic properties of graphene and T graphene: a theoretical approach. *Indian J. Phys.* **2017**, *91*, 1541. [CrossRef]
47. Kubo, R. Statistical-Mechanical Theory of Irreversible Processes. I. General Theory and Simple Applications to Magnetic and Conduction Problems. *J. Phys. Soc. Jpn.* **1957**, *12*, 570. [CrossRef]
48. Viswanath, V.; Müller, G. Recursion method in quantum spin dynamics: The art of terminating a continued fraction. *J. Appl. Phys.* **1990**, *67*, 5486. [CrossRef]
49. Muller, G.; Viswanath, V. *The Recursion Method: Application to Many-Body Dynamics*; Springer; Berlin, Germany, 1994.
50. Gagliano, E.R.; Balseiro, C.A. Dynamical Properties of Quantum Many-Body Systems at Zero Temperature. *Phys. Rev. Lett.* **1987**, *59*, 2999. [CrossRef] [PubMed]
51. Viswanath, V.S.; Zhang, S.; Müller, G.; Stolze, J. Zero-temperature dynamics of the one-dimensional XXZ and t-J models: A weak-coupling continued-fraction analysis. *Phys. Rev. B* **1995**, *51*, 368. [CrossRef] [PubMed]
52. Viswanath, V.; Müller, G. The recursion method applied to the T=0 dynamics of the 1D s=1/2 Heisenberg and XY models. *J. Appl. Phys.* **1991**, *70*, 6178. [CrossRef]
53. Mookerjee, A. A new formalism for the study of configuration-averaged properties of disordered systems. *J. Phys. C Solid State Phys.* **1973**, *6*, L205. [CrossRef]
54. Mookerjee, A. Averaged density of states in disordered systems. *J. Phys. C Solid State Phys.* **1973**, *6*, 1340. [CrossRef]
55. Mookerjee, A. Fermion-field theory and configuration averaging. *J. Phys. C Solid State Phys.* **1975**, *8*, 1524. [CrossRef]
56. Mookerjee, A. Structure of the scattering diagrams for conductivity in random binary alloys and the self-consistent CCPA. *J. Phys. C Solid State Phys.* **1986**, *19*, 193. [CrossRef]
57. Mookerjee, A. Cluster approximations to response functions in disordered systems and macroscopic conservation laws. *J. Phys. C Solid State Phys.* **1976**, *9*, 1225. [CrossRef]
58. Chowdhury, S.; Jana, D.; Sadhukhan, B.; Nafday, D.; Baidya, S.; Saha-Dasgupta, T.; Mookerjee, A. Configuration and self-averaging in disordered systems. *Indian J. Phys.* **2016**, *90*, 649. [CrossRef]
59. Haydock, R.; Nex, C.M.M. Densities of states, moments, and maximally broken time-reversal symmetry. *Phys. Rev. B* **2006**, *74*, 205121. [CrossRef]
60. Luchini, M.; Nex, C. A new procedure for appending terminators in the recursion method. *J. Phys. C Solid State Phys.* **1987**, *20*, 3125. [CrossRef]
61. Beer, N.; Pettifor, D.G. The Recursion Method and the Estimation of Local Densities of States. In *The Electronic Structure of Complex Systems*; Phariseau, P., Temmerman, W.M., Eds.; NATO ASI Series (Series B: Physics); Springer: Boston, MA, USA, 1984; Volume 113.
62. Pettifor, D.G.; Weaire, D.L. *The Recursion Method and Its Applications: Proceedings of the Conference, Imperial College, London, England, 13–14 September 1984*; Springer Science, Business Media: Berlin/Heidelberg, Germany, 2012; Volume 58.
63. Lee, C. New Approach to Study Critical Dynamics by Using Continued Fraction Representation. *J. Phys. Soc. Jpn.* **1989**, *58*, 3910. [CrossRef]
64. Haydock, R.; Heine, V.; Kelly, M. Electronic structure based on the local atomic environment for tight-binding bands. *J. Phys. C Solid State Phys.* **1972**, *5*, 2845. [CrossRef]
65. Ebert, H. The Munich SPR-KKR Package. Available online: https://www.ebert.cup.uni-muenchen.de/kkr/kkrlicense/ (accessed on 11 November 2022).
66. Perdew, J.P.; Burke, K.; Ernzerhof, M. Generalized Gradient Approximation Made Simple. *Phys. Rev. Lett.* **1996**, *77*, 3865. [CrossRef]
67. Liechtenstein, A.; Katsnelson, M.; Gubanov, V. Exchange interactions and spin-wave stiffness in ferromagnetic metals. *J. Phys. Met. Phys.* **1984**, *14*, L125. [CrossRef]
68. Uppsala Atomistic Spin Dynamics (Uppasd). Available online: http://www.physics.uu.se/uppasd (accessed on 11 November 2022).
69. Sasıoğlu, E.; Friedrich, C.; Blügel, S. Strong magnon softening in tetragonal FeCo compounds. *Phys. Rev. B* **2013**, *87*, 020410. [CrossRef]
70. Jakobsson, A.; Sasıoğlu, E.; Mavropoulos, P.; Ležaić, M.; Sanyal, B.; Bihlmayer, G.; Blügel, S. Tuning the Curie temperature of FeCo compounds by tetragonal distortion. *Appl. Phys. Lett.* **2013**, *103*, 102404. [CrossRef]
71. Lynn, J.W. Temperature dependence of the magnetic excitations in iron. *Phys. Rev. B* **1975**, *11*, 2624. [CrossRef]
72. Mook, H.A.; Nicklow, R.M. Neutron Scattering Investigation of the Magnetic Excitations in Iron. *Phys. Rev. B* **1973**, *7*, 336. [CrossRef]
73. Halilov, S.; Perlov, A.; Oppeneer, P.; Eschrig, H. Magnon spectrum and related finite-temperature magnetic properties: A first-principle approach. *Europhys. Lett.* **1997**, *39*, 91. [CrossRef]
74. Oogane, M.; Wakitani, T.; Yakata, S.; Yilgin, R.; Ando, Y.; Sakuma, A.; Miyazaki, T. Magnetic Damping in Ferromagnetic Thin Films. *Jpn. J. Appl. Phys.* **2006**, *45*, 3889. [CrossRef]
75. Muniz, R.B.; Mills, D.L. Theory of spin excitations in Fe(110) monolayers. *Phys. Rev. B* **2002**, *66*, 174417. [CrossRef]
76. Costa, A.T.; Muniz, R.B.; Cao, J.X.; Wu, R.Q.; Mills, D.L. Magnetism of an Fe monolayer on W(110). *Phys. Rev. B* **2008**, *78*, 054439. [CrossRef]
77. Zakeri, K.; Peixoto, T.; Zhang, Y.; Prokop, J.; Kirschner, J. On the preparation of clean tungsten single crystals. *Surf. Sci.* **2010**, *604*, L1. [CrossRef]

78. Ikeda, S.; Miura, K.; Yamamoto, H.; Mizunuma, K.; Gan, H.; Endo, M.; Kanai, S.; Hayakawa, J.; Matsukura, F.; Ohno, H. A perpendicular-anisotropy CoFeB–MgO magnetic tunnel junction *Nat. Mater.* **2010**, *9*, 721. [CrossRef]
79. Liu, L.; Pai, C.; Li, Y.; Tseng, H.; Ralph, D.; Buhrman, R. Spin-Torque Switching with the Giant Spin Hall Effect of Tantalum. *Science* **2012**, *336*, 555. [CrossRef] [PubMed]
80. Liu, L.; Lee, O.J.; Gudmundsen, T.J.; Ralph, D.C.; Buhrman, R.A. Current-Induced Switching of Perpendicularly Magnetized Magnetic Layers Using Spin Torque from the Spin Hall Effect. *Phys. Rev. Lett.* **2012**, *109*, 096602.[CrossRef] [PubMed]